Published in final edited form as:
Inhal Toxicol. 2014 August ; 26(10): 588–597. doi:10.3109/08958378.2014.937882.

The Acute Exposure Effects of Inhaled Nickel Nanoparticles on Murine Endothelial Progenitor Cells

Eric N Liberda[1,2], **Azita K Cuevas**[1], **Qingshan Qu**[1], and **Lung Chi Chen**[1]

[1]New York University School of Medicine, Department of Environmental Medicine, Tuxedo, NY

[2]School of Occupational and Public Health, Ryerson University, Ontario, Canada

Abstract

Introduction—The discovery of endothelial progenitor cells (EPCs) may help to explain observed cardiovascular effects associated with inhaled nickel nanoparticle exposures such as increases in vascular inflammation, generate reactive oxygen species, alter vasomotor tone, and potentiated atherosclerosis in murine species.

Methods—Following an acute whole body inhalation exposure to 500μg/m^3 of nickel nanoparticles for 5 hrs, bone marrow EPCs from C57BL/6 mice were isolated. EPCs were harvested for their RNA or used in a variety of assays including chemotaxis, tube formation, and proliferation. Gene expression was assessed for important receptors involved in EPC mobilization and homing using RT-PCR methods. EPCs, circulating endothelial progenitor cells (CEPCs), circulating endothelial cells (CECs), and endothelial microparticles (EMPs) were quantified on a BD FACSCalibur to examine endothelial damage and repair associated with the exposure.

Results and Conclusions—Acute exposure to inhaled nickel nanoparticles significantly increased both bone marrow EPCs as well as their levels in circulation (CEPCs). CECs were significantly elevated indicating that endothelial damage occurred due to the exposure. There was no significant difference in EMPs between the two groups. Tube formation and chemotaxis, but not proliferation, of bone marrow EPCs was impaired in the nickel nanoparticle exposed group. These results coincided with a decrease in the mRNA of receptors involved in EPC mobilization and homing. This data provides new insight into how an acute nickel nanoparticle exposure to half of the current Occupational Safety & Health Administration permissible exposure limit may adversely affect EPCs.

Keywords

Nanoparticles; endothelial progenitor cells; nickel; inhalation

Correspondence address to: Lung Chi Chen, Ph.D., Department of Environmental Medicine, NYU School of Medicine, 57 Old Forge Road, Tuxedo, NY 10987, lung-chi.chen@nyumc.org.

Declaration of interest statement: All authors declare they have no competing interests.

Introduction

As the nanotechnology industry continues to grow, the concerns for human health exposures from these nanomaterial containing products also increases. In response to this concern, the US federal budget for nanomaterial environmental, health, and safety was increased from 67.9 million dollars to 116.9 million dollars from 2008 to 2011 (Sargent JF, 2011). In 2009 alone, products incorporating nanomaterials into their technologies represented $254 billion across the global economy (M.C. Roco, C.A. Mirkin, and M.C. Hersam, 2010). However, as the nanotechnology industry continues to grow, and as nanomaterials continue to be incorporated into consumer goods, the lack of comprehensive toxicological assessments may lead to increased health risks due to consumer exposure from nanomaterial containing goods as well as from worker exposure during manufacturing processes. The growing use of nanosized materials in consumer products has raised concerns about their potential adverse health effects (Maynard et al., 2006). The physical and chemical properties of nanomaterials that make them attractive for use in industrial and consumer goods, namely their small size and high surface area, are also the same properties that make them a concern for health researchers (Maynard et al., 2011). It is abundantly evident that the research, development, and production of nanosized materials have outpaced their ability to be evaluated in a timely manner and therefore, there is an ever growing need to properly assess and quantify the health effects associated with nanosized materials.

Stemming from the observed cardiovascular effects of high concentrations of nickel in air pollution, several studies have attempted to gain an understanding into how nickel nanoparticles may exacerbate cardiovascular disease (Cuevas et al., 2010; Gillespie et al., 2010; Kang et al., 2011; Liberda et al., 2010; Lippmann et al., 2006). The specific properties of nickel nanoparticles, namely high surface area, high surface energy, high magnetism, and low melting and boiling points earmark this compound for growing use in the nano-market (Zhao et al. 2009) and there has been at least one reported death due to inhalation of nickel nanoparticles (Phillips et al. 2009) and other adverse health effects associated with exposure (Journeay et al. 2014). We have previously reported that sub-chronic inhalation of nickel hydroxide ($Ni(OH)_2$) nanoparticles causes both numerical alterations and functional impairment of bone marrow resident endothelial progenitor cells (EPCs) (Liberda et al., 2010). Until recently, it was thought that vasculogenesis, the process by which new blood vessels form, only occurred in the embryonic phase (Doyle et al. 2006). However, it has been shown that EPCs have a high capacity for vascular repair and have thus become an area of great research interest (Zampetaki et al. 2008). Since these cells are thought to be responsible for endothelial homeostasis in the cardiovascular system, any alteration in their number or function may have profound adverse health effects (Povsic and Goldschmidt-Clermont, 2008). For instance, it has been established that circulating EPC number is inversely related with the Framingham Risk Score for heart disease (Hill et al., 2003). In this study, we use a robust set of fluorescent markers, additional functional assessments, RT-PCR methods, proteomic analysis, and *in vitro* and *in vivo* exposures to explore the adverse effects associated with an acute whole body nickel nanoparticle exposure rather than a sub-chronic exposure. The focus on an acute study was performed as others have reported exposure duration to elicit different cellular responses.

Methods

Animals and Animal Care

Six week old C57BL/6 male mice were purchased from Jackson Laboratory, Bar Harbor, ME and housed at the New York University (NYU) animal facility (American Association for Laboratory Animal Science certified) in polycarbonate cages. The cages held autoclaved corncob bedding and were placed under a laminar flow hood equipped with a HEPA filter contained in a temperature and humidity controlled room. Food and water was provided *ad libitum* except during the exposure period. Light and dark cycles were maintained on 12 hour intervals. Prior to exposure, mice were acclimatized for 2 weeks. All animal procedures used in this study were conducted under an approved protocol by the New York University School of Medicine Institutional Animal Care and Use Committee (NYU IACUC).

Nanoparticle Exposure System

Mice were placed in metal compartmentalized whole body exposure chambers for 5 hours and received either HEPA filtered air treatments or approximately 500 $\mu g/m^3$ of nickel nanoparticles. This value represents one half of the current Occupational Safety & Health Administration (OSHA) permissible exposure limit (1 mg/m^3) and is also a midpoint in our previous study (Liberda et al., 2010). A Palas GFG-100 nanoparticle generator produced solid particles in an arc furnace containing opposing nickel electrodes which were discharged into a reagent grade argon carrier gas and mixed with purified air and oxygen before being delivered to the exposure chamber as described by Liberda et al. (2010) and Gillespie et al. (2010).

Particle characteristics were previously reported (Gillespie et al., 2010). Briefly, the nickel nanoparticles were characterized for size and number concentration using a Differential Mobility Analyzer (DMA, model TSI 3071) coupled to a condensation nucleus counter (CNC, model TSI 2010). X-ray photonelectron spectroscopy (XPS) was used to confirm the nickel species being generated and transmission electron microscopy (TEM) was used to verify size. The nickel exposure concentrations were determined using gravimetric methods with an ultra-sensitive microbalance placed in a temperature and humidity controlled weighing room.

Tissue Collection

Mice were sacrificed 30 min post-exposure and 12 hrs post-exposure to allow sufficient air changeover in the exposure chamber such that no nanoparticles would be present and to assess the effects of a recovery period, respectively. At time of sacrifice, mice were injected with 10% v/v pentobarbital (300 μl), wiped clean with ethanol, and weighed. Sacrifice between control and exposure groups was performed since it took 6 to 7 mins to process each mouse. Blood was collected with 0.5M EDTA rinsed syringes and placed on ice in tubes containing 100 μl of EDTA. The lower abdominal aorta and the aortic arch were excised and the external fat removed under a dissecting microscope before being frozen in liquid nitrogen. In order to collect bone marrow EPCs, the fur was removed from the lower extremities of the body and the entire leg was removed from the hip joint. Muscle tissue was removed with scissors and by gently rubbing and pulling with tissues. The isolated bones,

the femur and tibia, were placed in PBS and transferred to a laminar flow hood in a cell culture facility where the epiphysis of both the tibia and femur were removed. The bone marrow was flushed with a 23G needle containing 1 ml PBS repeatedly. After flushing, the cells were centrifuged and resuspended in 1ml of PBS before being placed above 1 ml of Histopaque-1083 (Sigma-Aldrich, USA) and spun at 300 × g for 20 mins with no brake. The buffy layer was gently removed with a bulb and pasture pipette and topped up to 5ml with EGM-2MV media before being counted on a hemocytometer. Cells were plated as required by the various assays on pre-coated 10 μg/ml human fibronectin tissue culture plates (Sigma-Aldrich, USA) and placed in an incubator at 37°C and 5% CO2 for 3-4 days to allow EPCs to adhere while other cells were removed. Media was changed every 3 days until the cells were used for the various experiments. Each EPC sample used in all experiments represented a single mouse.

Flow Cytometry

The discovery of circulating EPCs by Asahara and colleagues (Asahara et al. 1997) reformed prevailing theories on angiogenesis and vasculogenesis, opened new doors to cell-based therapies and provided insight into a variety of disease states. EPCs are stored in the bone marrow and are mobilized to circulation by SDF-1α signals where they home to sites of injury by following VEGF gradients (Jevon et al. 2008). Once mobilized into circulation, EPCs are termed circulating endothelial progenitor cells (CEPCs). Circulating endothelial cells (CECs) are mature endothelial cells that become detached from injured vessels and are typically found in low quantities in healthy individuals (Blann and Pretorius 2006; Boos et al. 2006; Gao et al. 2008; Goon et al. 2005). Individuals with pathological conditions associated with endothelial damage, such as atherosclerosis and diabetes, have levels of CECs that statistically exceed the average of healthy individuals. In addition, upon endothelial cell injury, vesicles are formed and released which have cell surface markers similar to endothelial cells but also reflect the cell status (activated, damaged or apoptotic). These vesicles are termed endothelial microparticles (EMPs; (Dignat-George and Boulanger 2011)). In addition to being markers of vascular injury (Heiss et al. 2008; Kaur et al. 2011; Pirro et al. 2006), EMPs may also be mediators of endothelial damage since it appears that they play a direct role in inflammation, thrombosis, and angiogenesis by controlling the release of cytokines and adhesins (Dignat-George and Boulanger 2011; Goon et al. 2006).

All cells (see below) were analyzed using a Becton Dickinson FACSCalibur system (Fluorescence-activated cell sorter flow cytometer) equipped with a 15 mW argon laser (488 nm) and a 17 mW HeNe laser (633 nm) in the New York University School of Medicine's Flow Cytometry Core. The FACSCalibur instruments has detectors for forward and side scatter and a minimum of 3 color channels excited by the 488 laser and one excited by the 633 laser.

A total of 20 mice were used in the flow cytometry experiments - 10 control and 10 nickel nanoparticle exposed. The methods were previously described in Liberda et al. (Liberda et al., 2010) with slight modification. Briefly, after ficoll separation and isolation of mononuclear cells, 1 million cells were blocked, stained with antibodies (Table 1; BD Biosciences) for 30 mins, washed with a FACS buffer solution, and fixed in 2%

paraformaldehyde (PFA). For CECs and circulating endothelial progenitor cell (CEPC) analysis, whole blood was first processed by lysing the red blood cells using FACS lysis solution (BD Biosciences, California) under vortex, and then stained, washed in a buffer solution and fixed in 2% PFA. EMPs were collected from plasma after a light 160 × g 10min spin to remove cell debris, followed by the transfer of 50 μl of plasma, and another 1400 × g 10 min spin to remove platelets before being stained for the antigens listed in Table 1. All cells except EMPs were strained using a 40 μm nylon mesh.

Due to a lack of consensus on a murine EPC phenotype in both bone marrow and whole blood, the bone marrow EPCs and CEPCs were quantified using SCA-1, VEGF-R2, and CD45 antigen and expressed as either SCA-1+/VEGF-R2+/CD-45−, SCA-1+/VEGF-R2+/CD-45+, or SCA-1+/VEGF-R2+ populations. CECs and EMPs from peripheral blood were assessed as being double positive for CD-146+/CD-31+. Table 1 summarizes the various phenotypes for the different cells analyzed.

Quantitative Real Time RT-PCR

RNA was isolated from cultured bone marrow EPCs (n=8) using the Qiagen RNeasy kit as per the manufacturer's instructions. A similar method was used for the aortic tissue (n=5) except that the samples were frozen in liquid nitrogen and smashed using a frozen block before being placed in the QIAshredder spin column. The isolated RNA was reverse transcribed into cDNA using the High Capacity Reverse Transcription Kit as per manufacturer's directions (Applied Biosystems, Foster City, CA). The relative mRNA levels were quantified using an Applied Biosystems 7900 Real-Time PCR Instrument (Applied Biosystems, Foster City, CA) with TaqMan® Gene Expression Assay primer/probe sets. Relative mRNA expression levels were calculated using the ΔΔCT method and normalized to the endogenous control gene, β-actin. The mRNA levels of the receptor for VEGF, VEGF-R2, and the receptor for SDF-1α, CXCR-4, were evaluated from bone marrow resident EPCs using RT-PCR. The abundance of ICAM-1, VCAM-1, and Connexin-43 were assessed in aortic tissue.

Circulating Plasma Protein Analysis

The plasma levels of VEGF and SDF-1α, proteins involved in the release of EPCs from the bone marrow and homing to sites of endothelial injury were evaluated using sensitive ELISA kits from Quantikine (Minneapolis, MN) as per the manufacturer's directions (n=8).

Endothelial Progenitor Cell Characterization

After EPCs were isolated from bone marrow they were plated 4×10^4 cells/well in an 8 well chamber slide containing 10 μg/ml human fibronectin (Sigma-Aldrich, USA). After 10 days in culture to plate off any other cells except for EPCs, the cells were washed with PBS and incubated with acLDL-DiI (10μg/ml) for 3 hours in an incubator. Following the acLDL staining, cells were washed with PBS and fixed with 4% paraformaldehyde in PBS for 10 minutes at room temperature. After washing with PBS, 0.1% Triton X-100 in PBS was placed in the chambers for 10 mins in order to permeabilize the cells. The chambers were then washed with PBS and blocked with 2% BSA for 30 minutes at room temperature. After blocking, cells were stained with Ulex-lectin for 3 hours at room temperature and then

washed with PBS before adding secondary Alexa-488 antibody. The cells were then washed with PBS, and the nuclei was stained with DAPI. EPCs were scored under a fluorescent microscope and considered positive if they contained both red (acLDL) and green (Ulex-lectin) with blue (DAPI) nuclei (Figure 1).

Cell Function Characterization

Three cellular function assays were performed; proliferation, tube formation, and chemotaxis. These assays represent the most important functions of EPCS; their ability to proliferate, their ability to form tubes (angiogenesis), and their ability to follow chemical signal stimuli (chemotaxis).

Proliferation—A cell proliferation ELISA was performed on bone marrow EPCs using a Roche Applied Science (Indianapolis, IN) assay kit according to the manufacturer's instructions with minor modifications. The bromodeoxyuridine (BrdU) incorporation assay was performed on naïve EPCs (ie. EPCs from unexposed mice) or EPCs from exposed and control mice after 10 days in culture and plated at a concentration of 2×10^4 cells/well in a fibronectin coated (10μg/ml) 96-well cell culture plate (n=10 for 0.5hr post-exposure and control group and n=5 for 12hr post-exposure and control group). Fifty ng/ml of VEGF was added to the wells and allowed to incubate for 24 hrs. Following this incubation, the BrdU was added to the wells for 2 hrs and BrdU incorporation was determined colorimetrically with horseradish peroxidate anti-BrdU antibody. Measurements were recorded on an ELISA plate reader at 370 nm less the 492 nm reference wavelength.

The ability of EPCs to migrate was assessed using a modified Boyden chamber assay. Before conducting assays, polyvinylpyrrolidone-free polycarbonate filter Transwell inserts (24 well, 8 μm pores; Transwell, USA) were incubated with fibronectin (10 μg/ml). The inserts were then placed in a 24-well plate containing 500 μl EGM-2MV medium with 50 ng/ml of VEGF. After 10 days in culture, the adherent EPCs were trypsinized and added to the upper chamber of the inserts in EGM-2MV medium (2×10^4 cells/insert; n=6 control, n=8 exposed for both 0.5 hr and 12 hr time points). Cells migrated from the upper to the lower chamber during a 24 hr period in an incubator set at 37°C with 5% CO2. Non-migratory cells were removed from the upper chamber by wiping the upper surface with an absorbent tip. Cells that migrated to the lower side of the Transwell insert were fixed for 1 min with methanol and stained with hematoxylin. After extensive PBS washing to remove excess hematoxylin, the number of cells that migrated were counted in three different representative high power (200×) fields per insert. The data was presented as number of cells migrated ± standard deviation.

Tube Formation—Ninety six well plates were coated with 50 μl of Matrigel (BD Biosciences, USA) and 2×10^4 EPCs were added to each well and placed in an incubator (37°C and 5% CO2) for 24 hrs (n=10 for both 0.5 hr and 12 hr time points). After 24 hrs in the incubator, each entire well was examined by light microscopy for the ability to form capillary-like structures. Only structures containing a minimum of 3 cells with endothelial capillary linkages were counted as tubes.

Plasma Exposure and Chelation Experiment

We previously reported that exposure to sub-chronic inhaled nickel nanoparticles were able to cause adverse effects in EPC number and function. Based on our previous dissolution studies (Kang et al. 2011b), and since the bone is perfused with blood, we hypothesized that either nickel ions that had translocated into the blood, or nickel induced unknown factors in blood plasma, were responsible for the observed effects. In order to test this hypothesis, cultured EPCs from the air control mouse (i.e. naïve mice) were serum starved for 1hr, and exposed to plasma from either nickel nanoparticle exposed mouse or a filtered air control mouse. The media used contained 0.5% serum, and the plasma was added at a concentration of 5% v/v. Upon incubation for 24 hours, tube formation, chemotaxis, and proliferation were assessed as described above.

In order to determine if the nickel compound or a plasma mediator was responsible for the observed functional deficits in the EPCs, TPEN (N,N,N′,N′-Tetrakis(2-pyridylmethyl)-ethylenediamine), a divalent chelator used in vitro to chelate a variety of divalent metals including nickel (McNulty and Taylor, 1999), was added at 20μM to filtered air control circulating EPCs for 1 hour. The media was then removed and the plasma exposure described above was repeated. It is important to note that the blood plasma was collected in EDTA, a chelating agent, but further chelation was used to ensure all divalent metal ions were removed.

Proteomic Analysis

Frozen plasma (−80°C) was sent to Applied Biomics (Hayward, CA) overnight on dry ice and analyzed as per the manufacturer. Briefly, the proteins were enriched, extracted, and labeled with Cy 2 and Cy 3 dye and run on an SDS-PAGE gel for a total of 3 gels. A merged image analyzed by GE Healthcare DeCyder ™ 2D Differential Analysis Software (v7.0) was used to identify proteins with the greatest abundance difference between control and exposure groups (minimum difference of +1.25 fold change cutoff).

Upon selection of which spots to analyze, the individual proteins were removed from the SDS–PAGE gel. The 2D spot was then washed multiple times, dried, and rehydrated in digestion buffer containing sequencing grade modified trypsin. The digested peptides were then extracted from the gel with an extraction buffer and shaking and desalted using C-18 Zip-tips (Millipore). The desalted peptides were mixed with an alpha-cyano-4-hydroxycinnamic acid matrix and spotted into wells of a matrix-assisted laser desorption/ionization (MALDI) plate. The mass spectra of the peptide in each sample were obtained using an Applied Biosystems Proteomics Analyzer matrix-assisted laser desorption/ionization–time of flight (MALDI-TOF) mass spectrometer. The identification of the proteins was based on peptide fingerprint mass mapping (using MS spectra from MALDI-TOF) and peptide fragmentation mapping (using MS/MS spectra). GPS Explorer software, equipped with MASCOT search engine, was used to identify proteins from primary sequence databases. After protein identification, a pathway analysis was performed on 42 proteins using the Database for Annotation, Visualization, and Integrated Discovery (DAVID v6.7; http://david.abcc.ncifcrf.gov/).

Statistical Analysis

Statistical analyses were conducted in GraphPad (v.5). A Student's t-test or a one-way analysis of variance (ANOVA) was performed on the data followed by the Student Neuman-Kuel post-hoc test. Probability values (p) less than 0.05 were considered significant. All error bars presented in figures represent standard deviation.

Results

Particle Characterization

Nickel nanoparticles generated for these experiments were previously characterized and reported by Gillespie and colleagues (Gillespie et al., 2010). TEM analysis and electrostatic classification found that the primary particles generated were 5 nm in size and that the count mean diameter agglomerated nanoparticle that entered the exposure chamber was 40 nm. Subsequent XPS analysis identified the spark generated nickel nanoparticles to be nickel (II) hydroxide ($Ni(OH)_2$) in its core and on its surface. The concentration of nickel nanoparticles delivered to the whole body exposure chamber was 537.1±76.43 $\mu g/m^3$.

In vitro EPC Characterization

EPCs were characterized after 10 days in culture as previously noted. This was done to confirm an EPC phenotype using fluorescent microscopy. No significant differences in baseline EPC number, quantified as double positive for acLDL and lectin, were found between the exposure and control group (n=10). An example image of the double positive stained cells has been provided in Figure 1A-C.

Bone Marrow Endothelial Progenitor Cell Functional Assessments

The results from the tube formation assay (Figure 2A) show that bone marrow EPC tube formation was significantly reduced in the nickel exposed mice group compared to the filtered air group. This reduction in EPC tube formation was significant at both the 0.5 hr post-exposure mouse group and in the 12 hr recovery (post-exposure) mouse group. Similar to the tube formation results, chemotaxis was significantly reduced in the nickel nanoparticle exposed group at both the 0.5 hr and 12 hr post-exposures (Figure 2B). However, unlike tube formation and chemotaxis, proliferation was not significantly different between the exposure and control groups in both the 0.5 hr and 12 hr post-exposure sacrifice groups (Figure 2C), although a non-significant decrease in the exposed group was observed.

Flow Cytometry Assessments

Flow cytometry data for CEPCs and bone marrow EPCs were analyzed in FlowJo (v.7.6.4) by gating on the lympho-mononuclear region of the forward and side scatter plots and then gating positive or negative for CD-45. This region was used as some studies suggest that both monocytes as well as lymphocytes have angiogenic potential (Shantsila et al., 2007; Shantsila et al., 2008; Shantsila et al., 2011). CECs were gated solely on the lymphocyte region and assessed by measuring double positive CD-31 and CD-146 cells while EMPs were gated on particles <1 μm for which the machine was calibrated using Sphereotech (Lake Forest, IL) beads of 0.53 μm, 1.26 μm, and 3.0 μm, and then measured as double

positive for CD-31 and CD-146. All phenotypes for all cells were significantly increased in the exposed group compared to the control except for EMPs. A summary of the FACS analysis findings is presented in Table 2.

Blood Plasma Analysis

The assessment of VEGF and SDF-1α in blood plasma was performed in order to determine if these signaling plasma proteins are present at increased or decreased levels after nickel nanoparticle exposure. Both 0.5hr and the 12hr exposure recovery plasma did not differ significantly from the control group (data not shown).

Quantitative Real Time RT-PCR Analyses

Quantitative real time RT-PCR was performed on bone marrow EPCs and total aorta (arch and lower abdominal aorta) at both 0.5hr and 12hr recovery exposure time points (Figure 3A, B). Compared to controls, bone marrow EPC VEGF-R2 and CXCR-4 were significantly downregulated at both time points, and Connexin-43 was significantly upregulated at both time points. When comparing the bone marrow EPC RT-PCR results, the data suggest that EPCs have a reduction in the expression of receptors involved in EPC release and homing, but an increase in gap junction expression after exposure *in vivo* exposure to inhaled nickel nanoparticles. The 12hr post recovery time point shows a significant increase in Connexin-43 mRNA as well as a non-significant return to baseline for VEGF-R2 and CXCR-4.

Aorta mRNA expression of genes related to early markers of atherosclerosis were assessed to determine if short exposures could elicit an early response in this tissue (Figure 3A). Surprisingly, monocytic chemotactic protein-1 (MCP-1) was significantly downregulated after 0.5 hr post-exposure sacrifice in the nickel group and returned to baseline 12 hrs post-exposure. This finding was tested several times and the data were consistently reproduced. No other genes were significantly different from the control group at either the 0.5 hr post-exposure or the 12 hr post-exposure time point.

Plasma and Chelation Functional Studies

The results from the *in vitro* treatment of naïve EPCs with plasma collected from filtered air control mice or nickel nanoparticle exposed mice with and without the divalent chelator TPEN are presented in Figure 4. Naïve EPCs exposed to nickel exposed plasma significantly reduced both chemotaxis (Figure 4A) and tube formation function (Figure 4B) of these cells both with and without TPEN. This finding suggested that nickel itself may not be the responsible compound for the observed effects, but rather, some nickel-induced plasma protein mediators may be the causal agent. Thus, in order to investigate what proteins may have been altered we performed a proteomic analysis of the blood plasma.

Blood Plasma Proteomics Studies

Based on the 3 SDS-PAGE gels, DeCyder™ analysis selected 42 protein spots with fold differences ±1.25 for further analysis and identification (Table 3). Of particular interest was the significant, and expected, upregulation of superoxide dismutase [Cu-Zn] and alpha-1-antitrypsin 1-5 precursor in the exposed group, indications of an inflammatory response. In

addition we observed a non-significant downregulation trend of transferrin. Thus, it is possible that that nickel, or a protein, may compete with iron during transferrin complexing. DAVID analysis suggested that exposure to nickel nanoparticles affected pathways associated with blood coagulation, hemostasis, and wound healing among other similar clusters.

Discussion

As noted, the concentration used in this study was approximately one half of the permissible exposure limit set by OSHA. Thus, in theory a worker could potentially be exposed for 8 hrs per day. Unfortunately there are no current exposure limits for nanoparticles and this remains an important issues to date as nanoparticle use in commercial goods and industrial uses is expected to increase. The adverse effects on the various cells are troubling as they occurred below current exposure limits. Similar to the CEPC findings in this study, Heiss et al. (Heiss et al., 2008) found that brief second hand smoke exposure caused these cells to be upregulated in circulating blood. Additionally, Gill et al. (Gill et al., 2001) found that following vascular trauma, CEPCs were also significantly upregulated in analyzed blood samples. More recently, Brook and colleagues found that an acute exposure to coarse mode particulate matter resulted in increases in CEPCs (Brook et al., 2013) but not circulating plasma VEGF; results that mirror our findings. Like the previous authors, we believe these findings are uniquely due to the acute nature of the exposures.

For instance, others found that longer duration exposures to inhaled CAPs and acrolein resulted in a decrease in CEPC number (O'Toole et al., 2010; Wheat et al., 2011). While these findings may be explained by the longer duration of the exposure studies, other factors such as concentration and type toxicant used in the study may also play a role. However, based on the current literature, we believe that prolonged exposure to certain toxicants and chronic disease states would ultimately exhaust bone marrow EPCs, inevitably reducing the CEPC population which help in repairing damaged endothelium. This hypothesis is bolstered by other studies which result in a decrease in CEPCs due to exposures or diseases of a chronic nature (eg. Balbarini et al., 2007; Niu et al., 2013; Sabatier et al., 2009. Our data suggest that an acute inhalation exposure to nickel nanoparticles results in sufficient endothelial trauma that EPCs are mobilized from the bone marrow into systemic circulation as evidenced by our enumeration of EPCs, CEPCs and CECs.

Haberzettl and colleagues showed that concentrated ambient particles caused a decrease in CEPCs which was attributed to specific effects on VEGF-induced mobilization (Haberzettl et al., 2012). Interestingly, while we found that plasma levels of VEGF and SDF-1α were not significantly different between control and exposure groups, gene expression of bone marrow EPCs was significantly downregulated for VEGF-R2 and CXCR-4, the two cellular receptors for VEGF and SDF-1 α. Similar to these findings, Cruz et al. (Cruz et al., 2005) found that exposure to a soluble nickel compound (nickel sulfate) caused a significant reduction of CXCR-4 expression in dendritic cells. Therefore, the homing and release signals for the bone marrow resident EPCs may be adversely affected with exposure which may ultimately affect the repair capacity of these cells. This data suggests that inhalation of nickel nanoparticles can cause bone marrow EPCs to lose their ability to sense proteins

required for release and homing. These findings were bolstered by our significant decrements in bone marrow EPC function, specifically chemotaxis and tube formation, which rely on these chemical signals. Michaud and colleagues also found that exposure to smoke caused a reduction in the chemotaxis potential and tube formation of EPCs (Michaud et al., 2006). The loss of EPC function is particularly concerning given their reparative role in the cardiovascular system.

With regards to the plasma exposure assay results, it is possible that nickel ions from the inhalation exposure may have translocated into the circulation or other proteins from the acute exposure may have been released and adversely affected bone marrow EPC function. Previous attempts by our group have shown that blood nickel levels cannot be distinguished above background levels and therefore we cannot use this method of quantitation (Kang et al., 2011). The results of *in vitro* treatment with plasma from nickel exposed mice suggested that certain components in the plasma collected from the nickel nanoparticle exposed mice, be it either nickel ions, plasma proteins, or other molecules such as archidonic acid metabolites may be driving these observed effects. Since nickel in blood plasma could not be ruled out as a causal agent for the observed effects, a chelation study was performed to determine the cause of the functional deficits. Both chemotaxis and tube formation showed significant deficits in the nickel plasma exposed group from the EPCs that were treated with the divalent chelator TPEN. These data suggested that nickel ions themselves may not play a role in the observed adverse effects, but that resulting circulating plasma proteins from the inhalation exposure may be the causal agent for the observed functional deficits in bone marrow EPCs.

Accordingly, proteomic analysis was performed on the plasma collected from both the exposed and control animals to determine which plasma proteins were up or downregulated and may be responsible for the observed effects of nickel exposure. The results from the proteomic analysis suggest that transferrin may be responsible for bringing nickel into the cell and perhaps altering the iron status of EPCs since it was found in reduced levels in plasma. This may be because nickel ions are either outcompeting Fe (III) for transferrin, or that nickel ions are binding to excess transferrin in plasma and entering the cell. Our proteomic results also found that in response to the nickel nanoparticle exposure, cellular oxidative defenses of the EPCs were elevated compared to filtered air controls.

In the aorta, MCP-1, a monocytic chemotactic protein, ICAM-1 and VCAM-1, both adhesion molecules, were selected for investigation due to their role in atherosclerosis plaque development (Blankenberg et al., 2003; Kitagawa et al., 2002; Libby, 2000; Nakashima et al., 1998). While ICAM-1 and VCAM-1 levels were both non-significantly altered by the exposure, we hypothesize that MCP-1 was significantly downregulated as a protective mechanism to prevent the early adhesion of monocytes in response to an acute endothelial injury.

The significant downregulation in the gene expression of important receptors involved in EPC release and homing (VEGF-R2 and CXCR-4) is also an important finding. These results may aid to elucidate why the EPCs from individuals who have been exposed to various toxicants may be functionally deficient. While the mechanism by which VEGF-R2

and CXCR-4 become downregulated is not known, these results help explain the loss of EPC function as assessed by tube formation and chemotaxis.

Conclusion

The interplay between damaged endothelium, measured as CECs and EMPs, and its ability to repair injury, measured as bone marrow EPCs and CEPCs, is important to understanding the effects of inhaled nickel nanoparticles. By discovering whether or not nickel nanoparticle exposure alters the number of these cells, we may gain a better understanding of the downstream cardiovascular effects observed by Kang et al (Kang et al., 2011). Homeostatic regulation of the endothelium is a complex process involving damage and repair. Alterations to this dynamic equilibrium result in the reduction of the ability of EPCs to repair damaged endothelium, whether it is by a reduction in cell number or in cellular function. In this study, an acute exposure to inhaled nickel nanoparticles caused increases in bone marrow EPCs, CEPCs, and CECs. This data adds to the body of literature illustrating that an acute exposure, and ensuing injury, may alter the gene expression of the cells and affect cell function. This is important not only from an occupational standpoint, but also from a public health perspective due to nickel laden air particles. Research to further understand the mechanisms by which nickel nanoparticles cause adverse health effects is still required. However, the work herein provides great insight into the effects associated their exposure as well as valuable insights into possible mechanisms of action.

Acknowledgments

The authors acknowledge grant support from NIEHS R01ES015495 (L Chen), R21ES016570 (Q Qu), P30 ES00260 (L Chen and Q Qu) and CIHR-DRA (E Liberda).

References

Balbarini A, Barsotti MC, Di Stefano R, Leone A, Santoni T. Circulating endothelial progenitor cells characterization, function and relationship with cardiovascular risk factors. Curr Pharm Des. 2007; 13:1699–713. [PubMed: 17584100]

Blankenberg S, Barbaux S, Tiret L. Adhesion molecules and atherosclerosis. Atherosclerosis. 2003; 170:191–203. [PubMed: 14612198]

Brook RD, Bard RL, Kaplan MJ, Yalavarthi S, Morishita M, Dvonch JT, et al. The effect of acute exposure to coarse particulate matter air pollution in a rural location on circulating endothelial progenitor cells: results from a randomized controlled study. Inhal Toxicol. 2013; 25:587–92. [PubMed: 23919441]

Cruz MT, Goncalo M, Paiva A, Morgado JM, Figueiredo A, Duarte CB, et al. Contact sensitizers downregulate the expression of the chemokine receptors CCR6 and CXCR4 in a skin dendritic cell line. Arch Dermatol Res. 2005; 297:43–7. [PubMed: 15924226]

Cuevas AK, Liberda EN, Gillespie PA, Allina J, Chen LC. Inhaled nickel nanoparticles alter vascular reactivity in C57BL/6 mice. Inhal Toxicol. 2010; 22(Suppl 2):100–6. [PubMed: 21142798]

Gill M, Dias S, Hattori K, Rivera ML, Hicklin D, Witte L, et al. Vascular trauma induces rapid but transient mobilization of VEGFR2(+)AC133(+) endothelial precursor cells. Circ Res. 2001; 88:167–74. [PubMed: 11157668]

Gillespie PA, Kang GS, Elder A, Gelein R, Chen L, Moreira AL, et al. Pulmonary response after exposure to inhaled nickel hydroxide nanoparticles: Short and long-term studies in mice. Nanotoxicology. 2010; 4:106–19. [PubMed: 20730025]

Haberzettl P, Lee J, Duggineni D, McCracken J, Bolanowski D, O'Toole TE, et al. Exposure to ambient air fine particulate matter prevents VEGF-induced mobilization of endothelial progenitor cells from the bone marrow. Environ Health Perspect. 2012; 120:848–56. [PubMed: 22418586]

Heiss C, Amabile N, Lee AC, Real WM, Schick SF, Lao D, et al. Brief secondhand smoke exposure depresses endothelial progenitor cells activity and endothelial function: sustained vascular injury and blunted nitric oxide production. J Am Coll Cardiol. 2008; 51:1760–71. [PubMed: 18452782]

Hill JM, Zalos G, Halcox JP, Schenke WH, Waclawiw MA, Quyyumi AA, et al. Circulating endothelial progenitor cells, vascular function, and cardiovascular risk. N Engl J Med. 2003; 348:593–600. [PubMed: 12584367]

Journeay WS, Goldman RH. Occupational handling of nickel nanoparticles: A case report. Am J Ind Med. DOI: 10.1002/ajim.22344.

Kang GS, Gillespie PA, Gunnison A, Moreira AL, Tchou-Wong KM, Chen LC. Long-term inhalation exposure to nickel nanoparticles exacerbated atherosclerosis in a susceptible mouse model. Environ Health Perspect. 2011; 119:176–81. [PubMed: 20864429]

Kang GS, Gillespie PA, Gunnison A, Rengifo H, Koberstein J, Chen LC. Comparative pulmonary toxicity of inhaled nickel nanoparticles; role of deposited dose and solubility. Inhal Toxicol. 2011b; 23(2):95–103. doi: 10.3109/08958378.2010.543440.

Kitagawa K, Matsumoto M, Sasaki T, Hashimoto H, Kuwabara K, Ohtsuki T, et al. Involvement of ICAM-1 in the progression of atherosclerosis in APOE-knockout mice. Atherosclerosis. 2002; 160:305–10. [PubMed: 11849652]

Libby P. Changing concepts of atherogenesis. J Intern Med. 2000; 247:349–58. [PubMed: 10762452]

Liberda EN, Cuevas AK, Gillespie PA, Grunig G, Qu Q, Chen LC. Exposure to inhaled nickel nanoparticles causes a reduction in number and function of bone marrow endothelial progenitor cells. Inhal Toxicol. 2010

Lippmann M, Ito K, Hwang JS, Maciejczyk P, Chen LC. Cardiovascular effects of nickel in ambient air. Environ Health Perspect. 2006; 114:1662–9. [PubMed: 17107850]

Roco MC, Mirkin CA, Hersam MC. Nanotechnology Research Directions for Societal Needs in 2020. 2010:610.

Maynard AD, Aitken RJ, Butz T, Colvin V, Donaldson K, Oberdorster G, et al. Safe handling of nanotechnology. Nature. 2006; 444:267–9. [PubMed: 17108940]

Maynard AD, Warheit DB, Philbert MA. The new toxicology of sophisticated materials: nanotoxicology and beyond. Toxicol Sci. 2011; 120(Suppl 1):S109–29. [PubMed: 21177774]

McNulty TJ, Taylor CW. Extracellular heavy-metal ions stimulate Ca2+ mobilization in hepatocytes. Biochem J. 1999; 339(Pt 3):555–61. [PubMed: 10215593]

Michaud SE, Dussault S, Haddad P, Groleau J, Rivard A. Circulating endothelial progenitor cells from healthy smokers exhibit impaired functional activities. Atherosclerosis. 2006; 187:423–32. [PubMed: 16288934]

Nakashima Y, Raines EW, Plump AS, Breslow JL, Ross R. Upregulation of VCAM-1 and ICAM-1 at atherosclerosis-prone sites on the endothelium in the ApoE-deficient mouse. Arterioscler Thromb Vasc Biol. 1998; 18:842–51. [PubMed: 9598845]

Niu J, Liberda EN, Qu S, Guo X, Li X, Zhang J, et al. The role of metal components in the cardiovascular effects of PM2.5. PLoS One. 2013; 8:e83782. [PubMed: 24386277]

O'Toole TE, Hellmann J, Wheat L, Haberzettl P, Lee J, Conklin DJ, et al. Episodic Exposure to Fine Particulate Air Pollution Decreases Circulating Levels of Endothelial Progenitor Cells. Circ Res. 2010

Phillips JI, Green FY, Davies JCA, Murray J. Pulmonary and systemic toxicity following exposure to nickel nanoparticles. Am J Ind Med. 2010; 53(8):763–767. [PubMed: 20623660]

Povsic TJ, Goldschmidt-Clermont PJ. Endothelial progenitor cells: markers of vas cular reparative capacity. Ther Adv Cardiovasc Dis. 2008; 2:199–213. [PubMed: 19124422]

Sargent JF. Nanotechnology and Environmental, Health, and Safety: Issues for Consideration. Congressional Research Service. Report number 7-5700.

Sabatier F, Camoin-Jau L, Anfosso F, Sampol J, Dignat-George F. Circulating endothelial cells, microparticles and progenitors: key players towards the definition of vascular competence. J Cell Mol Med. 2009; 13:454–71. [PubMed: 19379144]

Shantsila E, Watson T, Lip GY. Antioxidant protection: yet another function of endothelial progenitor cells? J Hum Hypertens. 2007; 21:343–6. [PubMed: 17314998]

Shantsila E, Watson T, Tse HF, Lip GY. New insights on endothelial progenitor cell subpopulations and their angiogenic properties. J Am Coll Cardiol. 2008; 51:669–71. [PubMed: 18261687]

Shantsila E, Wrigley B, Tapp L, Apostolakis S, Montoro-Garcia S, Drayson MT, et al. Immunophenotypic characterization of human monocyte subsets: possible implications for cardiovascular disease pathophysiology. J Thromb Haemost. 2011; 9:1056–66. [PubMed: 21342432]

Wheat LA, Haberzettl P, Hellmann J, Baba SP, Bertke M, Lee J, et al. Acrolein Inhalation Prevents Vascular Endothelial Growth Factor-Induced Mobilization of Flk-1+/Sca-1+ Cells in Mice. Arterioscler Thromb Vasc Biol. 2011

Zhao J, Shi X, Castranova V, Ding M. Occupational toxicology of nickel and nickel compounds. J Environ Pathol Toxicol Oncol. 2009; 28(3):177–208. [PubMed: 19888907]

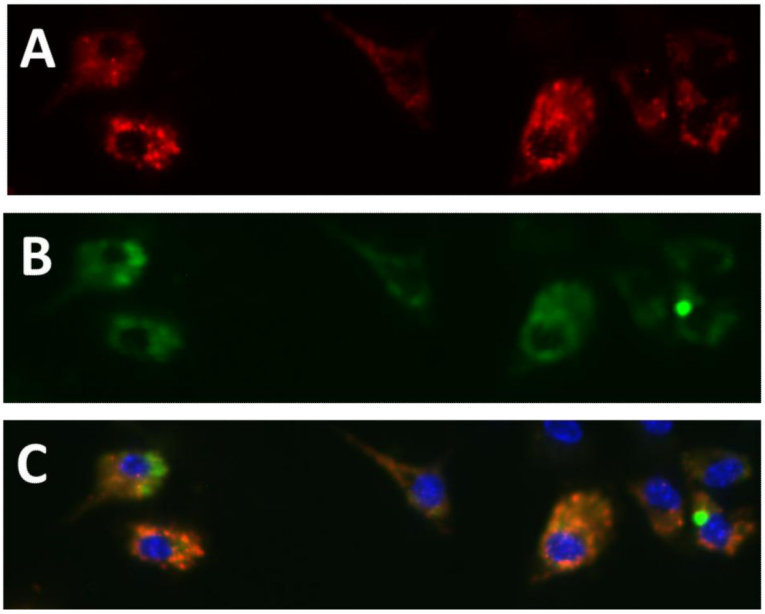

Figure 1.
Example of double positive (acLDL and Ulex-Lectin) cultured EPCs. (A) acLDL stain (B) Ulex-lectin stain (C) Double positive cells (combination of A and B) with blue DAPI nuclear stain.

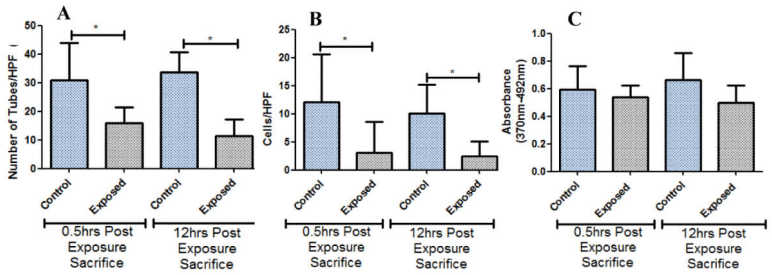

Figure 2.

(A) Tube formation results for 0.5 hr and 12 hr post-exposure sacrifices at 200x magnification. (B) Chemotaxis results for 0.5 hr and 12 hr post-exposure sacrifices. (C) Proliferation results for 0.5 hr and 12 hr post-exposure sacrifices. * denotes significance (n=8).

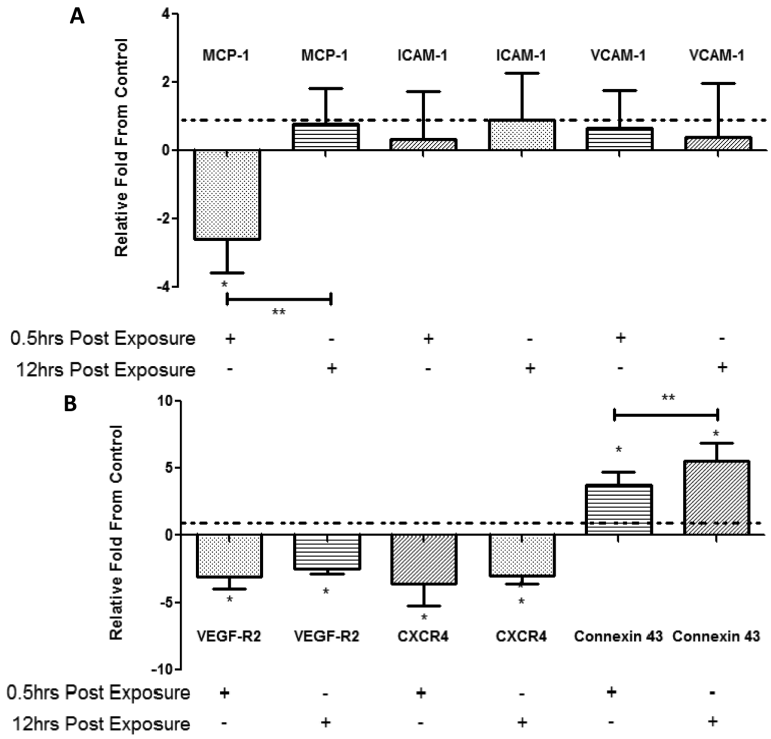

Figure 3.

(A) RT-PCR analysis results from cultured EPCs relative to control (dashed line) for 0.5 hr and 12 hr post-exposure sacrifices. (B) RT-PCR results from mouse aorta relative to control (dashed line) for 0.5 hr and 12 hr post-exposure sacrifice.*=significantly difference from control. **=significantly different from 0.5hr post-exposure sacrifice (n=10)

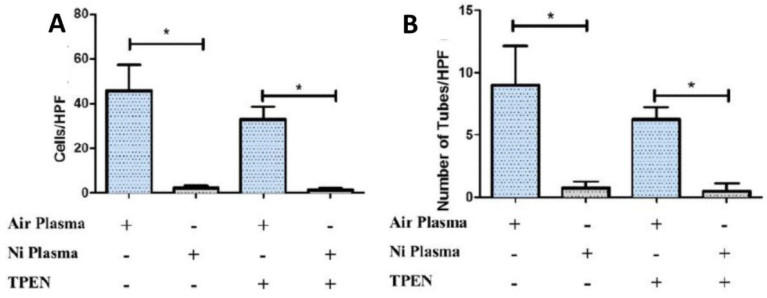

Figure 4.

(A) Chemotaxis results after chelation (TPEN [N,N,N′,N′-Tetrakis(2-pyridylmethyl)-ethylenediamine], a divalent chelator) and plasma exposure. (B) Tube formation results after chelation and plasma exposures. * denotes significance (n=8).

Table 1

Summary of Cell Phenotypes Assessed

Cell Phenotype
Bone Marrow EPCs
SCA-1+/VEGF-R2+/CD45−
SCA-1+/VEGF-R2+/CD45+
SCA-1+VEGF-R2+
Circulating EPCs
SCA-1+/VEGF-R2+/CD45−
SCA-1+/VEGF-R2+/CD45+
SCA-1+/VEGF-R2+
Circulating Endothelial Cells
CD31+/CD146+
Endothelial Microparticles
CD31+/CD146+

Table 2

Summary of FACS Analysis

Cell Analyzed	Direction of Change Compared to Control	*p* Value
Bone Marrow EPCs		
SCA-1+/VEGF-R2+/CD45−	Increase in number	0.006
SCA-1+/VEGF-R2+/CD45+	Increase in number	0.009
SCA-1+/VEGF-R2+	Increase in number	0.006
Circulating EPCs		
SCA-1+/VEGF-R2+/CD45−	Increase in number	0.038
SCA-1+/VEGF-R2+/CD45+	Increase in number	0.00005
SCA-1+/VEGF-R2+	Increase in number	0.00009
Circulating Endothelial Cells		
CD31+/CD146+	Increase in number	0.0004
Endothelial Microparticles		
CD31+/CD146+	--	0.758

-- denotes no significant directional change

Table 3

Protein ID of all 42 Spots by Mass Spectroscopy

Assigned ID	Protein ID	*p*value	Av. Ratio: exposure / control
1	alpha-fetoprotein	0.0083	−1.33
2	Serpinalc protein	0.037	1.29
3	sulfated glycoprotein-2 isoform 2	0.011	−1.29
4	Serpinalc protein	0.01	1.42
5	alpha-1-antitrypsin 1-5 precursor	0.047	1.43
6	Apoa4 protein	0.002	−1.26
7	Serpinalc protein	0.061	1.28
8	GUGU alpha	0.079	1.26
9	plasminogen, isoform CRA_a	0.0049	−1.31
10	serum albumin	0.057	1.34
11	fibrinogen beta chain precursor	0.091	−1.41
12	fibrinogen beta chain precursor	0.13	−1.60
13	fibrinogen beta chain precursor	0.19	−1.44
14	fibrinogen beta chain precursor	0.31	−1.34
15	transferrin	0.084	−1.26
16	fibrinogen, alpha polypeptide isoform 2	0.18	−1.35
17	fibrinogen, alpha polypeptide isoform 2	0.31	−1.31
18	fibrinogen, gamma polypeptide	0.15	−1.35
19	fibrinogen, gamma polypeptide	0.18	−1.45
20	fibrinogen, gamma polypeptide	0.18	−1.42
21	Igk protein	0.062	−1.84
22	immunoglobuhn J chain precursor	0.0062	1.35
23	albumin	0.0067	2.32
24	peroxiredoxin-2	0.07	1.76
25	peroxiredoxin-2	0.067	2.00
26	Apoal protein	0.094	1.70
27	purine nucleoside phosphorylase	0.071	1.62
28	immunoglobuhn kappa-chain VK-1	0.32	2.81
29	(P07724) Serum albumin precursor	0.034	1.44
30	Chain A, Crystal Structure Of The Anti-Bax Monoclonal Antibody 6a7 And A Bax Peptide.	0.79	−1.37
31	fibrinogen, alpha polypeptide isoform 2	0.062	1.77
32	unnamed protein product	0.016	1.95
33	creatine kinase M-type	0.015	2.95
34	carbonic anhydrase 2	0.075	1.70
35	carbonic anhydrase 2	0.089	1.84
36	carbonic anhydrase 2	0.085	1.57
37	carbonic anhydrase 1	0.056	1.80
38	Chain A, Structure Of Fab 7dl 1 From A Neutrahzing	0.18	1.46

Assigned ID	Protein ID	*p*value	Av. Ratio: exposure / control
	Antibody Against The Poxvirus LI Protein		
39	mCG20828*	0.032	1.40
40	superoxide dismutase [Cu-Zn]	0.21	2.27
41	hypothetical protein LOC210940 *	0.84	1.62
42	TD and POZ domain-containing protein 3*	0.12	1.81